



# Inhibition of the AP-1/TFPI2 axis contributes to alleviating cerebral ischemia/reperfusion injury by improving blood–brain barrier integrity

Yue Cao<sup>1,2</sup> · Ruixian Xing<sup>2</sup> · Qiushi Li<sup>2</sup> · Yang Bai<sup>2</sup> · Xuewen Liu<sup>2</sup> · Buxian Tian<sup>2</sup> · Xin Li<sup>1</sup>

Received: 1 March 2024 / Accepted: 23 August 2024  
© The Author(s) under exclusive licence to Japan Human Cell Society 2024

## Abstract

Reperfusion after cerebral ischemia leads to secondary damage to the nervous system, called cerebral ischemia/reperfusion injury (CIRI). The blood–brain barrier (BBB) consists of endothelial cells and tight junction (TJ) proteins, and its disruption aggravates CIRI. Two GSE datasets identified Tissue Factor Pathway Inhibitor 2 (TFPI2) as a differentially upregulated gene ( $\text{Log}_2\text{FC} > 1$ ,  $p < 0.01$ ) in the cerebral cortex of ischemic rats, and TFPI2 affects angiogenesis of endothelial cells. Moreover, genes (c-Jun, c-Fos, FosL1) encoding subunits of Activator Protein-1 (AP-1), a transcription factor involved in IRI, were highly expressed in ischemic samples. Thus, the effects of the AP-1/TFPI2 axis on CIRI were explored. We determined increased TFPI2 expression in the cerebral cortex of rats receiving middle cerebral artery occlusion (MCAO) for 90 min and reperfusion (R) for 48 h. Then AAV2-shTFPI2 particles ( $5 \times 10^{10}$  vg) were injected into the right lateral ventricle of rats 3 weeks before MCAO/R. TFPI2 knockdown decreased infarct size and neuronal injury in ischemic rats. It improved BBB integrity, demonstrated by reduced FITC-dextran leakage in brain tissues of MCAO/R-operated rats. Furthermore, it increased the expression of TJ proteins (Occludin, Claudin-5, TJP-1) in the cerebral cortex of rats with CIRI. Consistently, we found that TFPI2 knockdown mitigated cell damage in mouse endothelial bEND.3 cells with oxygen and glucose deprivation (ODG) for 6 h and reoxygenation (R) for 18 h (ODG/R) treatment. High co-expression of c-Jun and c-Fos significantly elevated TFPI2 promoter activity. c-Jun knockdown inhibited TFPI2 expression in OGD/R-treated bEND.3 cell. Collectively, our findings demonstrate that inhibition of the AP-1/TFPI2 axis alleviates CIRI.

**Keywords** Cerebral ischemia/reperfusion injury · Blood–brain barrier · Tight junction · Tissue factor pathway inhibitor 2 · Activator protein-1

## Introduction

Cerebral ischemia is a cerebrovascular disease with high morbidity and mortality, taking a toll on the life quality and span of patients [1, 2]. The pathogenesis of cerebral ischemia is complicated and it remains challenging despite a lot of efforts. Restoration of blood-flow supply to ischemic brain tissue is a common treatment after cerebral ischemia [3],

providing a valuable opportunity for the survival of neurons [4]. However, reperfusion results in undesired consequences, known as cerebral ischemia/reperfusion injury (CIRI), for the nervous system, including neuronal apoptosis, microglia activation, and inflammatory responses [5]. Furthermore, it is worth noting that vascular endothelial injury plays an important role in CIRI [6]. Vascular endothelial cells connected by tight junction (TJ) proteins form the crucial part of the blood–brain barrier (BBB) [7]. CIRI induces vascular endothelial injury and thereby aggravates BBB disruption, which was associated with the extent of inflammation during CIRI [8]. BBB disruption was proposed to interact with microglia activation and neuronal apoptosis [9, 10]. Preservation of BBB integrity was discovered to contribute to functional recovery after ischemia [11]. Therefore, improvement of BBB integrity might help for alleviating CIRI.

✉ Xin Li  
lixin@126.com

<sup>1</sup> Department of Neurology, The Second Hospital of Tianjin Medical University, Tianjin, People's Republic of China

<sup>2</sup> Department of Neurology, The First Affiliated Hospital of Jinzhou Medical University, Jinzhou, People's Republic of China

Based on two GSE datasets (GSE33725 and GSE97537) that contain gene expression profiles in the cerebral cortex of rats after cerebral ischemia and reperfusion or sham operation, we found that Tissue Factor Pathway Inhibitor 2 (TFPI2) was aberrantly upregulated in ischemic samples. TFPI2 is a Kunitz-type serine protease inhibitor mainly expressed by endothelial cells [12]. A large body of literature has demonstrated that TFPI2 took part in the development of several diseases such as cancer progression [13], and diabetes [14]. Nevertheless, the exact role of TFPI2 in CIRI has not been well studied previously. Ivanciu et al. reported that overexpression of TFPI2 inhibited migration and angiogenesis of endothelial cells [15]. Upregulation of TFPI2 expression was related to impaired angiogenesis of human umbilical vein endothelial cells [16]. These previous studies have pointed out the possibility that TFPI2 affects the development of CIRI through modulating the BBB permeability. How TFPI2 impacts CIRI and whether the underlying mechanism was mediated by BBB require to be further explored.

Activator Protein-1 (AP-1) is an important nuclear transcriptional activator and it is a heterodimer complex consisting of the JUN family (c-Jun, JunB, and JunD) and the FOS family (c-Fos, FosB, FosL1, and FosL2) [17, 18]. The promoter region of genes containing 12–0-tetradecanoyl-phorbol-13-acetate (TPA)-responsive elements (TREs, 5'-TGAG/CTCA-3') or cAMP-responsive elements (CRE, 5'-TGACGTCA-3') could be bound by AP-1, which promotes activation of gene transcription [19]. Similarly, the increased expression of c-Jun, c-Fos, and FosL1 was observed both in the GSE33725 and GSE97537 datasets. The c-Jun expression was usually upregulated in the injured nervous system [20]. Dai et al. revealed that focal CIRI induced high c-Jun and c-Fos protein levels in the cortex of rats, and the blockage of AP-1 activity exhibited beneficial effects [21]. Activated AP-1 after myocardial IRI was reported by Zingarelli et al. [22]. DNA binding activity of AP-1 and JunD protein levels was significantly increased after liver IRI [23]. These findings indicated a strong association between AP-1 and IRI. Several subunits of the AP-1 complex were predicted to bind to the promoter region of TFPI2 by the JASPAR database. Therefore, we supposed that AP-1 regulated the transcriptional activity of TFPI2 and further affected CIRI development.

In the present study, we investigated the role of TFPI2 knockdown and the transcriptional regulatory effect of AP-1 on TFPI2 after CIRI by loss-of-function experiments. Our results provide evidence that the inhibition of the AP-1 complex decreased the TFPI2 expression, alleviating the development of CIRI.

## Materials and methods

### The bioinformatics analysis of gene expression in rats with MCAO surgery

To explore the novel therapeutic target of CIRI treatment, GSE33725 and GSE97537 were downloaded from the Gene Expression Omnibus (GEO) of the NCBI database for bioinformatics analysis. Genes with  $|\text{Log}_2\text{FC}| \geq 1$  and  $p$  value  $< 0.05$  were determined as differentially expressed genes (DEGs) in the current study.

### MCAO rat model

Male Sprague–Dawley (SD) rats (8–10 weeks old) (Changsheng biotechnology, Liaoning, China) were subjected to middle cerebral artery occlusion (MCAO) surgery by suture-occluded method according to a previous protocol [24]. Briefly, after 1 week of adaptation, rats were anesthetized and incised along the midline of the neck to expose the right common carotid artery (CCA), internal carotid artery (ICA), and external carotid artery (ECA). A 4.0 monofilament nylon suture was inserted into ICA along CCA to achieve MCAO. Then the filament was removed after 90 min of occlusion for reperfusion. Eventually, rats were sacrificed after reperfusion of different times (6 h, 12 h, 24 h, or 48 h). Rats that suffered the same surgery but without occlusion were used as controls.

To explore the role of TFPI2 in CIRI, rats were injected with the recombinant adeno-associated virus (AAV) 2 (pAAV-CMV-U6) carrying shTFPI2 ( $5 \times 10^{10}$  vg in 5  $\mu\text{L}$  for each rat) using a 36-gauge glass cannula connected to a 10  $\mu\text{L}$  of syringe (0.2  $\mu\text{L}/\text{min}$ ). The injection location was located at 1.0 mm posterior to bregma, 2.0 mm lateral to midline on the right, and 3.5 mm below the skull surface. The recombinant AAV2 carrying non-targeting shRNA was used as the negative control. At 3 weeks after injection, rats that suffered the MCAO and 48 h of the reperfusion model were scored for neurologic deficits according to a widely used method [25]. Assessment of neurologic deficit score was performed by the investigator blinded to the experimental groups. The detailed scoring criteria are shown in Table S1. Evans blue (2%) was administered to rats at the dose of 4 mL/kg by tail-vein injection 3 h before euthanasia. One mL of FITC-dextran (50 mg/mL) was injected into the tail vein of rats to evaluate the permeability of the blood–brain barrier (BBB) according to the previously described [26]. After 30 min of injection, rats were euthanized and their brain tissues were collected for further use.

A total of 275 rats were used in the current study, of which 203 were used for the establishment of the

MCAO/R model. The mortality rate of rat MCAO/R model was 13.8%. Not all surviving MCAO/R-treated rats were included in the animal study. The exclusion criteria for surviving rats with MCAO/R treatment are as follows: subarachnoid hemorrhage and no observed ischemic pathologic changes using a microscope.

### **Tetrazolium Chloride (TTC) staining**

Fresh brain tissues were frozen at  $-20^{\circ}\text{C}$  for 3 h and cut into 5 serial coronal sections. Then brain sections were removed into culture dishes and fully stained with 2% TTC solution in a thermostatic incubator at  $37^{\circ}\text{C}$  under the dark condition for 15 min. After being turned over, sections were stained by TTC solution again for 15 min. Brain tissues were photographed to represent infarct size. Finally, infarct size analysis was performed by the investigator blinded to the experimental groups.

### **Evans blue and FITC-dextran extravasation**

Evans blue and FITC-dextran extravasation were used to evaluate BBB integrity. For Evans blue leakage, fresh brain tissues were removed from rats after heart perfusion with normal saline and photographed. Subsequently, brain tissues were frozen at  $-20^{\circ}\text{C}$  for 3 h, cut into 5 serial coronal sections, and photographed. For FITC-dextran leakage, fixed brain tissues were successively immersed into 20% and 30% sucrose solutions for dehydration. After OCT embedding, brain tissues were frozen-sectioned into  $10\ \mu\text{m}$  slices, which were subjected to antigen retrieval under high-temperature and low-fire conditions for 10 min. Blocked brain tissues were immune-labeled by CD31 (a marker for vascular endothelial cells) antibody (1:50) (Santa Cruz, California, USA) at  $4^{\circ}\text{C}$  overnight and Goat anti-mouse IgG-Cy3 (1:1000) (Proteintech, Hubei, China) at room temperature (RT) for 60 min successively. After DAPI (Aladdin, Shanghai, China) counterstain and treatment with an antifading-mounting medium (Solarbio, Beijing, China), images were captured by a microscope (BX53, OLYMPUS, Japan).

### **Quantitative real-time polymerase chain reaction (qRT-PCR)**

Tissues or cells were treated with TRIZOL reagent (BioTeke, Beijing, China) for isolation of total RNA. Subsequently, the RNA concentration was determined spectrophotometrically using NANO 2000 (Thermo, Massachusetts, USA). Complementary DNA was obtained by transcribing total RNA and it was used to run SYBR Green-based PCR on Exicycler 96 system (BIONEER, South Korea). The SYBR Green qRT-PCR conditions are as follows:  $95^{\circ}\text{C}$  for 5 min, and then 40 cycles of  $95^{\circ}\text{C}$  for 10 s,  $60^{\circ}\text{C}$  for 10 s, and  $72^{\circ}\text{C}$

for 15 s, followed by melting curve analysis. The mRNA levels of specific genes were determined using the  $2^{-\Delta\Delta\text{CT}}$  method and normalized by  $\beta$ -actin. BeyoRT™ II M-MLV reverse transcriptase was purchased from Beyotime (Shanghai, China). The RNase inhibitor was purchased from Biosharp (Anhui, China). SYBR Green and PCR MasterMix were purchased from Solarbio (Beijing, China). A detailed description of primer sequences used for qRT-PCR is shown in Table S2.

### **Western blot analysis**

Tissues or cells were treated with RIPA buffer (Proteintech, Hubei, China) for total protein isolation. Then, the protein concentration was determined by a BCA Protein Concentration Detection Kit (Proteintech, Hubei, China). Total protein was separated by SDS-PAGE and transferred to PVDF membranes (Thermo, Massachusetts, USA). Skim milk solution (5%) prepared with Tris-buffered saline Tween 20 (TBST) buffer was used to treat membranes for the blockage of non-specific binding sites. Then, membranes were incubated with primary antibodies overnight at  $4^{\circ}\text{C}$  and secondary antibodies for 40 min at  $37^{\circ}\text{C}$ , successively. After color development by Ultrasensitive ECL Detection Kit (Proteintech, Hubei, China), protein bands were visualized by Tanon-5200 (Shanghai, China).  $\beta$ -actin (Proteintech, Hubei, China) was used as the loading control. HRP-conjugated Affinipure Goat Anti-Rabbit IgG and HRP-conjugated Affinipure Goat Anti-Mouse IgG were purchased from Proteintech (Hubei, China). Antibodies against Occludin, Claudin-5, TJP-1, TFPI2, c-Jun, p-c-Jun, c-Fos, and FosL1 were purchased from Affinity (Jiangsu, China). A detailed description of antibodies used for western blot is shown in Table S3.

### **Immunofluorescence staining**

Fixed cells were permeated with 0.1% Triton X-100 (Beyotime, Shanghai, China) for 30 min at RT. For double immunofluorescence analysis, brain slices ( $5\ \mu\text{m}$ ) were prepared after dehydration with gradient ethanol and paraffin embedding. They were then treated with xylene solution for dewaxing and gradient ethanol solution for rehydration, and boiled using antigen retrieval solution for antigen retrieval. After being blocked with 1% BSA solution at RT for 15 min, cells or brain slices were subjected to primary antibody incubation overnight at  $4^{\circ}\text{C}$ , followed by secondary antibody incubation at RT (60 min for single-plex immunofluorescence staining and 90 min for multiplex immunofluorescence staining). Afterward, cells or brain slices were stained with DAPI (Aladdin, Shanghai, China), and mounted with an antifading-mounting medium (Solarbio, Beijing, China). Images of immunofluorescence staining were captured by a microscope (BX53, OLYMPUS, Japan). Antibodies against Occludin

and TFPI2 were purchased from Affinity (Jiangsu, China). CD31 antibody was purchased from Santa Cruz (California, USA). Goat anti-rabbit IgG-FITC, Goat anti-rabbit IgG-Cy3, and Goat anti-mouse IgG-Cy3 were purchased from Protein-tech (Hubei, China). A detailed description of antibodies used for immunofluorescence staining is shown in Table S4.

### Nissl staining

Paraffin-embedded brain tissues were cut into slices (5  $\mu\text{m}$ ) and subjected to dewaxing and rehydration. Subsequently, brain slices were covered with 0.5% cresyl violet solution for 10 min at RT. Then 0.25% glacial acetic acid prepared with 95% ethanol solution was used for color differentiation. After being dehydrated with a gradient ethanol solution, cleared with xylene, and mounted with neutral gum, brain slices were observed by a microscope (BX53, OLYMPUS, Japan). Cresyl violet was purchased from Sinoreagent (Shanghai, China). Glacial acetic acid was purchased from Chemreagent (Tianjin, China).

### Transmission electron microscopy

Cerebral cortex samples were fixed with 2.5% glutaraldehyde (Servicebio, Hubei, China), post-fixed with 1% OsO<sub>4</sub> (Ted Pella, Germany), and dehydrated with gradient ethanol and anhydrous acetone (Sinoreagent, Shanghai, China). After that, they were subjected to infiltration with acetone/812-embedding agents (Structure Probe Inc., Pennsylvania, USA) (1:1) at 37 °C for 2–4 h, and with acetone/812-embedding agent (1:2) at 37 °C overnight, followed by treatment with the pure 812-embedding agent at 37 °C for 5–8 h. Polymerization of embedding resin was accomplished by 48 h of baking at 60 °C. Ultra-thin slices (60–80 nm) were prepared and placed in 150-mesh copper grids, which were stained with 2% uranyl acetate in alcoholic solution for 8 min in the dark condition and 2.6% lead citrate solution for 8 min in the absence of carbon dioxide. Dried copper meshes were observed under a transmission electron microscope (H-7650, Hitachi, Japan).

### Brain-water content

After euthanasia, brain tissues of rats were removed and weighed immediately. Then brain tissues were dried until the weight remained constant. Brain-water content was calculated by the following formula:  $[(\text{wet weight}-\text{dry weight})/\text{wet weight}] \times 100\%$ .

### Cell culture, transfection, and treatment

Brain-derived Endothelial cells.3 (bEnd.3) cells were purchased from iCell Bioscience (Shanghai, China) and cultured with Dulbecco's Modified Eagle Medium (DMEM) supplemented with 10% fetal bovine serum (FBS) in an incubator at 37 °C under an atmosphere of 5% CO<sub>2</sub>. To mimic CIRI in vitro, bEnd.3 cells were cultured in the oxygen and glucose deprivation (OGD) environment (glucose-free Earle's solution, 94% N<sub>2</sub>, 1% O<sub>2</sub>, 5% CO<sub>2</sub>) for 6 h, followed by the reoxygenation (R) environment (DMEM, 95% air, 5% CO<sub>2</sub>) for 18 h. For gene knockdown, bEnd.3 cells were transfected with siRNAs targeting TFPI2 or c-Jun using Lipo3000 (Invitrogen, Massachusetts, USA) for 48 h. Non-targeting siRNA was used as the normal control. For gene expression at a high level, bEnd.3 cells were co-transfected with pcDNA3.1-c-Jun and pcDNA3.1-c-Fos plasmids (1:1) for 48 h. Empty pcDNA3.1 plasmid was used as the control. The siRNAs targeting TFPI2 and c-Jun were purchased from JTSBIO (Hubei, China). The pcDNA3.1-c-Jun and pcDNA3.1-c-Fos plasmids were synthesized by YouBio (Hunan, China).

### Cell viability

Cell viability was performed using the Cell counting kit-8 (CCK-8) kit (KeyGEN, Jiangsu, China) according to the manufacturer's protocol. Briefly, bEnd.3 cells were seeded into 96-well plates (5  $\times$  10<sup>3</sup> cells/per well). After transfection, cells were subjected to OGD/R treatment. The 10  $\mu\text{L}$  of CCK-8 detection solution was added to each well. Then plates were cultured in a 5% CO<sub>2</sub> incubator at 37 °C for 2 h. Following that, the optical density (OD) value at the wavelength of 450 nm was detected by a microplate reader (800TS, BIOTEK, USA).

### Measurement of lactate dehydrogenase (LDH) activity

LDH activity in the supernatant of the cell culture medium was determined by the Lactate dehydrogenase assay kit (Nanjing Jiancheng, Jiangsu, China) according to the manufacturer's protocol.

### Measurement of transepithelial electrical resistance (TEER)

The TEER value of the bEnd.3 monolayer was measured by an electrical resistance meter (Millicell ERS-2, Millipore, Germany) to assess the integrity of BBB. Briefly, cells (5.0  $\times$  10<sup>4</sup>/each well) were seeded into 12 mm cell culture filter inserts (LABSELECT-Cat#14,212, Anhui, China), which were inserted into 12-well plates and cultured until the cell monolayer reached confluence. Then, cells were transfected with



siRNA targeting TFPI2 and subjected to OGD/R treatment. Wells only containing the culture medium were used as the blank control. Electrodes of the electrical resistance meter were connected to two sides of the cell monolayer to measure the TEER value of the cell monolayer in the culture chamber.

### Prediction of the binding relationship

An online analysis website JASPAR (<https://jaspar.elixir.no/>) was used to predict the binding site of subunits of the AP-1 complex in the promoter region of TFPI2, for exploring whether the TFPI2's effects were regulated by the AP-1 complex. First, the promoter sequence of TFPI2 in the FASTA format was obtained using the UCSC Genome Browser (<https://genome.ucsc.edu/>). Then, JASPAR was used to predict the presence or absence of binding sites.

### Dual luciferase reporter assay

TFPI2 promoter (−2000~ +45 bp) was inserted into the pGL3-Basic vector to produce the TFPI2 promoter report construct (pGL3-TFPI2<sup>PRO</sup>). An empty pGL3-Basic vector was used as the control. Hela cells purchased from iCell Bioscience (Shanghai, China) were cultured with Minimum Essential Medium (MEM) supplemented with 10% FBS in a 5% CO<sub>2</sub> incubator at 37 °C. After 24 h of culture, Hela cells were co-transfected with the empty plasmid (pcDNA3.1) or pcDNA3.1-c-Jun or/and pcDNA3.1-c-Fos plasmids along with pGL3-TFPI2<sup>PRO</sup> using Lipo3000. Luciferase activity was measured using a Dual Luciferase Reporter Gene Assay Kit (KeyGEN, Jiangsu, China) and calculated by the following formula: Firefly luciferase activity/Renilla luciferase activity. The pGL3-Basic vector was purchased from Hunan Fenghui Biotechnology (Hunan, China).

### Statistical analysis

Quantitative data were displayed in the form of mean ± standard deviation (SD). GraphPad Prism 9 was used for statistical analysis. Significant differences between two groups were determined by two-tailed Student's t test or Mann–Whitney test. Kruskal–Wallis with Dunn's post-hoc test or one-way ANOVA with the Tukey post-hoc test was used for three or more groups. Statistical significance was set at  $p < 0.05$ .

## Results

### High TFPI2 expression in cerebral ischemic samples

To find a novel target for alleviating CIRI, we first analyzed DEGs from two GSE datasets (GSE33725 and GSE97537). By overlapping DEGs from cortex samples of rats after 2 h and 6 h of MCAO surgery in the GSE33725 dataset, we

determined 55-upregulated and 2-downregulated genes. Subsequently, the intersection of DEGs between two GSE datasets was performed and the results displayed that there were 25-upregulated genes and no downregulated genes. Among these upregulated DEGs, we further identified TFPI2 as the potential therapeutic target for CIRI because of its close relationship with endothelial cells (Fig. 1a). The expression profile of TFPI2 in GSE33725 and GSE97537 datasets was shown in Fig. 1b. TFPI2 mRNA level was significantly increased in ischemic samples compared with that in sham-operated samples.

### TFPI2 expression was increased after CIRI

To investigate the role of TFPI2 in CIRI, rats were subjected to MCAO/R surgery to stimulate CIRI in vivo (Fig. 2a). Brain tissues of rats were collected and stained by TTC to evaluate infarct size. Representative images of TTC staining manifested that ischemic rats had obvious cerebral infarction (the region with pale white) on the right side of brain tissues (Fig. 2b). Quantitative analysis for TTC-stained brain tissues also confirmed that MCAO/R promoted the increase of infarct area in brain tissues of rats compared with sham operation (Fig. 2c). The TFPI2 mRNA and protein expression in the cerebral cortex were detected after ischemia for 90 min and reperfusion with different time (6, 12, 24, and 48 h). The MCAO/R group showed a higher TFPI2 expression than the Sham group. The longer reperfusion time led to a higher TFPI2 level (Fig. 2d, e). Double immunofluorescence staining was performed to locate the TFPI2 expression in vascular endothelial cells of the cerebral cortex. It revealed that CIRI led to increased TFPI2 expression in vascular endothelial cells (Fig. 2f).

### TFPI2 knockdown blunted CIRI

Similar to the expression profile of TFPI2 in two GSE datasets, we also validated the higher TFPI2 expression in the ischemic samples. Afterward, we carried out the loss-of-function of TFPI2 experiments in vivo to explore the effects of TFPI2 on CIRI (Fig. 3a). After the MCAO/R operation, neurologic function of rats was assessed by neurologic deficit scoring in which higher scores represents more severe function damage. In comparison with sham-operated rats, ischemic rats exhibited marked neurologic function impairment while TFPI2 knockdown threw light on the unfavorable situation (Fig. 3b). The beneficial effect of TFPI2 knockdown on infarct size caused by MCAO/R was evidenced by images of TTC staining and its quantitative analysis (Fig. 3c, d). A successful knockdown of TFPI2 in the cerebral cortex of MCAO/R-operated rats was demonstrated by the

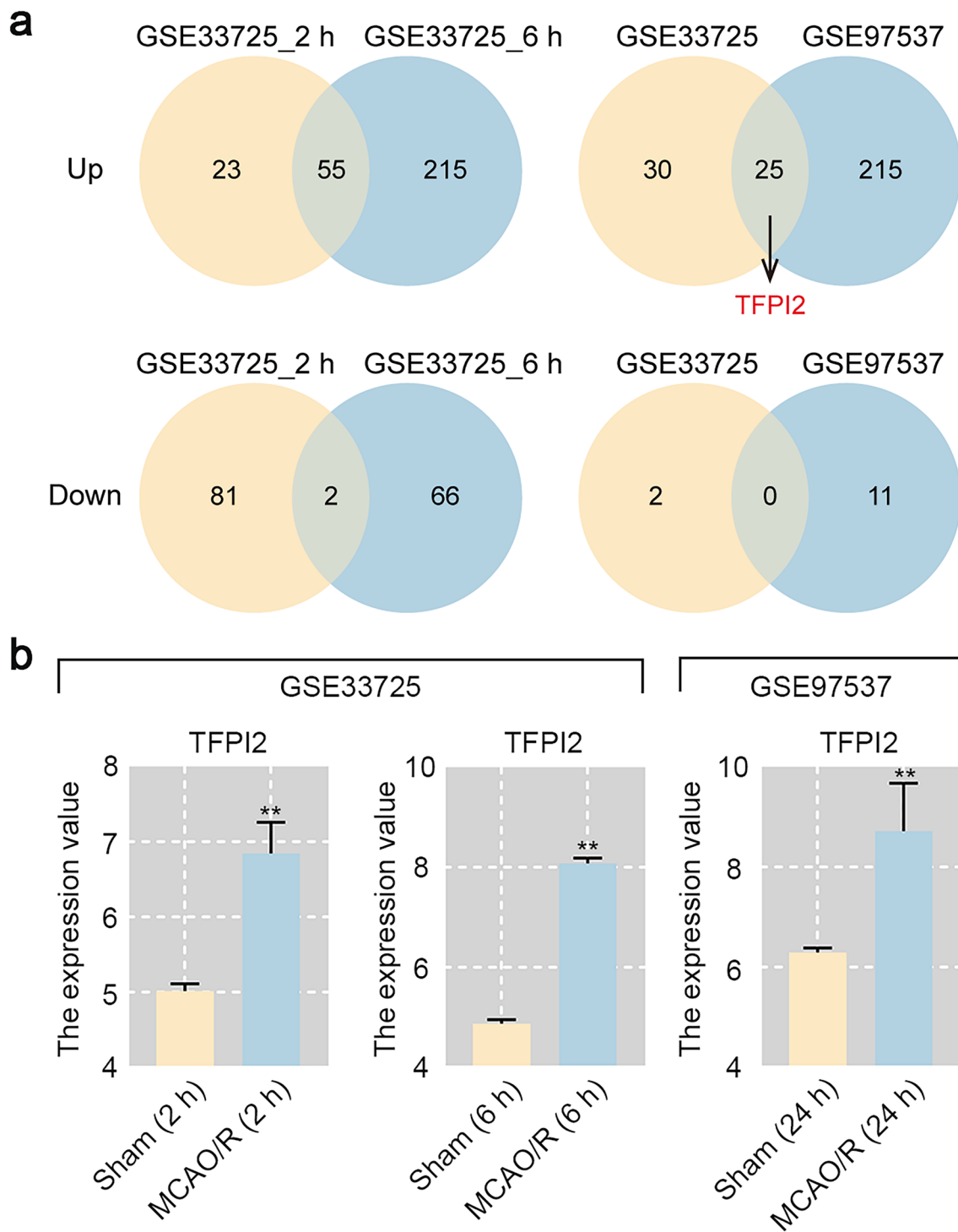


**Fig. 1** TFPI2 is identified as a candidate gene in cerebral ischemia/reperfusion injury (CIRI). **a** Venn diagrams show differentially expressed genes (DEGs) shared between GSE33725 and GSE97537.

**b** The expression profile of TFPI2 from GSE33725 and GSE97537.  $**p < 0.01$  versus the Sham group

decreased mRNA and protein levels of TFPI2 after injection of AAV2 carrying shTFPI2 (Fig. 3e, f). In addition, neuronal morphology in the cerebral cortex of rats was identified by Nissl staining. Nissl bodies were decreased in neurons in the

MCAO/R group, but TFPI2 knockdown showed an opposite trend (Fig. 3g).

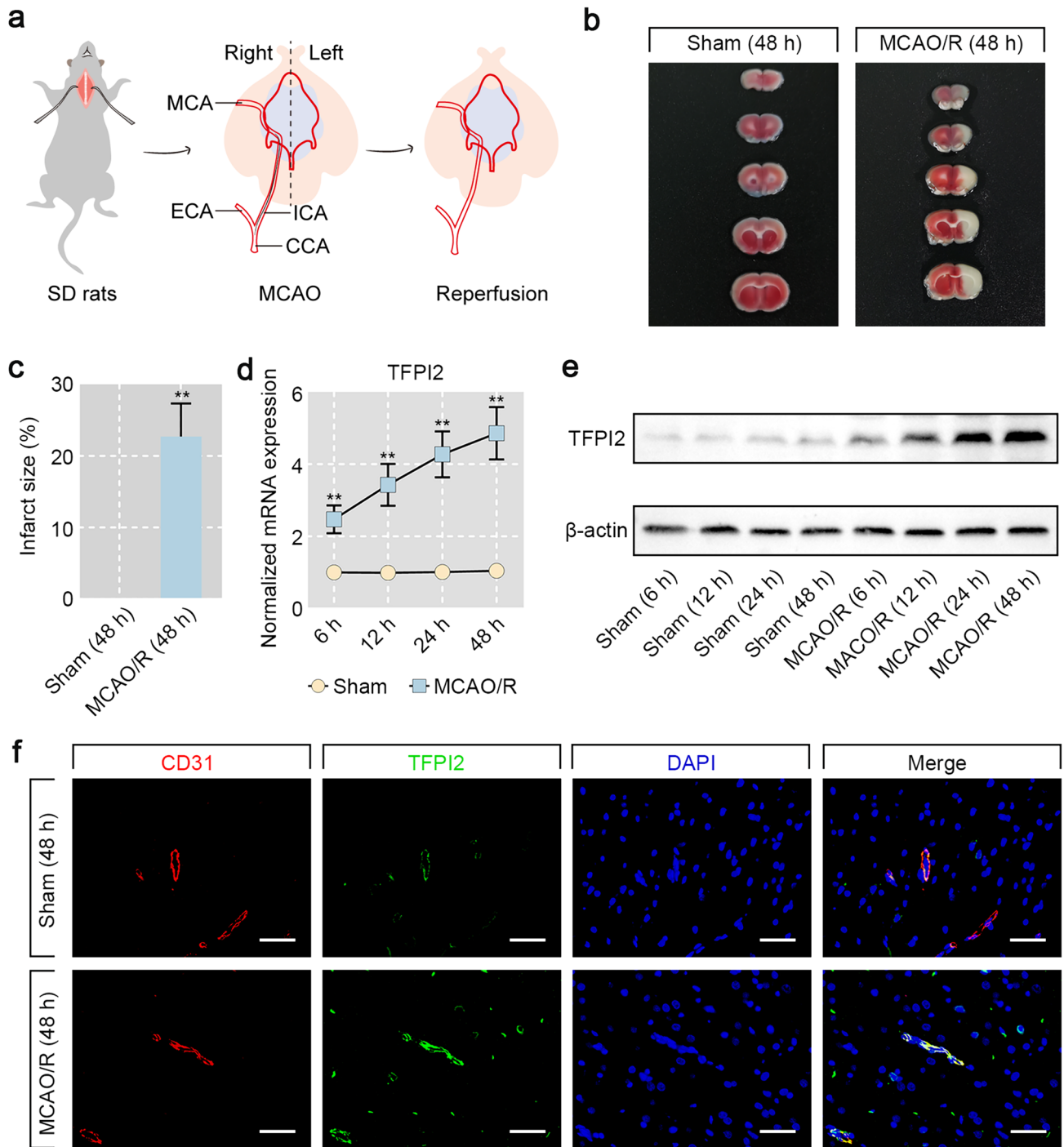


**Fig. 2** TFPI2 is highly expressed in rats with CIRI. **a** The schematic diagram of middle cerebral artery occlusion (MCAO) and reperfusion (R) treatment in rats. **b** Images of TTC staining display cerebral infarction of rats (n=6). **c** Quantitative analysis of infarct size indicated by TTC staining (n=6). **d** The mRNA expression of TFPI2 in cerebral cortex of rats after sham surgery or MCAO following different

ent time of R (6, 12, 24, or 48 h) (n=6). **e** The protein level of TFPI2 in cerebral cortex of rats after sham surgery or MCAO following different time of R (6, 12, 24, or 48 h) (n=6). **f** Images of double immunofluorescence staining locate TFPI2 expression in endothelial cells (n=6). Scale bar = 50 μm. \*\*p < 0.01 versus the Sham group

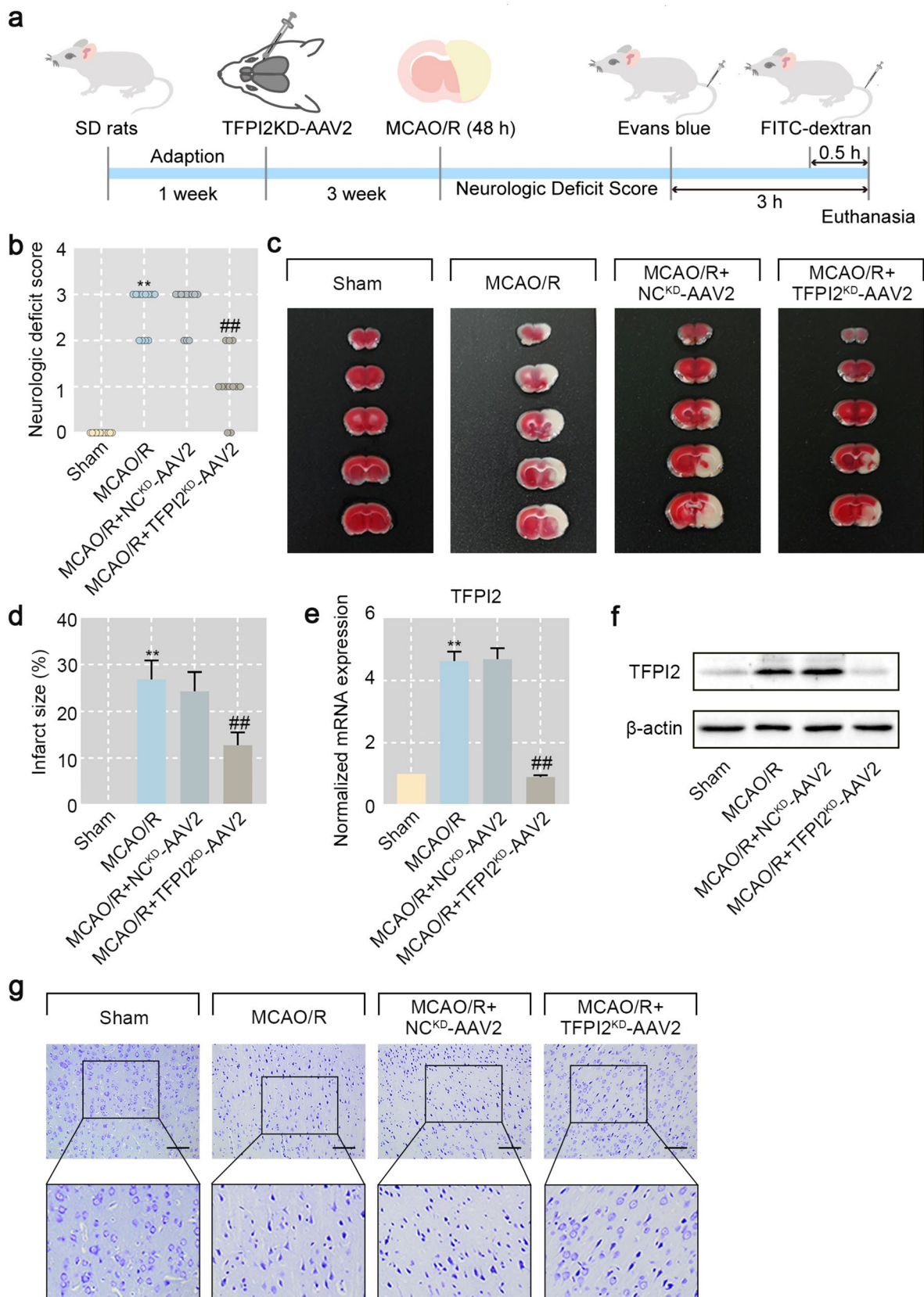




**Fig. 3** TFPI2 knockdown alleviates CIRI in rats. **a** The schematic diagram for the timeline of rats receiving AAV2-mediated TFPI2 knockdown, MCAO/R treatment, Evans blue and FITC-dextran injection. **b** Neurologic deficit scores visualize neurologic function of rats ( $n=12$ ). **c** Images of TTC staining display cerebral infarction of rats. **d** Quantitative analysis of infarct size indicated by TTC staining ( $n=6$ ). **e** The mRNA expression of TFPI2 in cerebral cortex of rats ( $n=6$ ). **f** The protein expression of TFPI2 in cerebral cortex of rats ( $n=6$ ). **g** Images of Nissl staining display neuronal damage in cerebral cortex of rats ( $n=6$ ). Scale bar = 100  $\mu\text{m}$ .  $**p < 0.01$  versus the Sham group,  $##p < 0.01$  versus the MCAO/R + NC<sup>KD</sup>-AAV2 group

### TFPI2 knockdown prevented BBB disruption

Damaged BBB integrity is an important pathologic event in CIRI. It contributes to the development of cerebral edema. The increased brain-water content in ischemic rats indicated that CIRI caused BBB leakage and further cerebral edema and it was reversed by TFPI2 knockdown (Fig. 4a). Evans blue and FITC-dextran cannot cross BBB under normal physiologic conditions and they were successively administered to rats before sacrifice by tail-vein injection. We then collected brain tissues and observed their extravasation to evaluate BBB integrity. And we noted that TFPI2 knockdown inhibited MCAO/R-induced Evans blue leakage in brain tissues of rats (Fig. 4b). For the FITC-dextran leakage assay, FITC-dextran was injected into rats via the tail vein. Subsequently, the cerebral cortex tissues of rats were collected and subjected to immunofluorescence staining with CD31 to mark the vascular endothelial barrier. After being imaged under a microscope, the FITC-dextran leakage through the BBB could be observed. Representative images showed that FITC-dextran passed through the BBB and distributed in the cerebral cortex of rats with CIRI, while its extravasation was mitigated by TFPI2 knockdown (Fig. 4c). Images derived from transmission electron microscopy revealed that MCAO/R treatment resulted in the disruption of tight junction, shown as the increased paracellular spaces, while TFPI2 knockdown restored the physical barrier between vascular endothelial cells (Fig. 4d).

### TFPI2 knockdown restored the expression of TJ proteins

TJ proteins are crucial components of BBB and their expression is tied to BBB integrity (Fig. 5a). Occludin, Claudin-5, and Tight Junction Protein 1 (TJP-1) are classic TJ proteins, and their expression levels were determined with western blot. Western blot assay showed that MCAO/R treatment reduced the expression of TJ proteins. However, rats treated with AAV2 encoding shTFPI2 had higher protein levels of Occludin, Claudin-5, and TJP-1 in the cerebral cortex compared with those treated with AAV2 encoding non-targeting shRNA (Fig. 5b). Then Occludin expression in vascular

endothelial cells was visualized by double immunofluorescence staining, which also revealed that TFPI2 knockdown inhibited the decrease in the Occludin expression caused by MCAO/R operation, consistent with the result of western blot (Fig. 5c).

### TFPI2 knockdown alleviated vascular endothelial cell damage after OGD/R treatment

OGD/R is a well-established method to simulate CIRI in vitro. After 48 h of transfection with siTFPI2, mouse brain microvascular endothelial cells bEND.3 were subjected to OGD/R treatment to explore the effects of TFPI2 knockdown on BBB disruption (Fig. 6a). The expression profile of TFPI2 was similar to that in in vivo experiments. Increased TFPI2 mRNA and protein levels in OGD/R-treated bEND.3 cells were downregulated by TFPI2 knockdown (Fig. 6b, c). OGD/R treatment reduced cell viability, but TFPI2 knockdown inhibited the alternation (Fig. 6d). LDH release into the culture supernatant was used to assay cell damage. TFPI2 knockdown inhibited OGD/R-induced LDH release of bEND.3 cells (Fig. 6e). TEER values of bEND.3 cell culture could indicate the tightness between endothelial cells. Disrupted endothelial barrier integrity caused by the OGD/R condition was reversed by TFPI2 knockdown, as revealed by the increased TEER value (Fig. 6f). Accordingly, western blot assay showed that the decreased protein levels of Occludin, Claudin-5, and TJP-1 were significantly elevated by TFPI2 knockdown in bEND.3 cells after OGD/R exposure (Fig. 6g). Immunofluorescence staining also confirmed that OGD/R-treated cells had a lower Occludin expression compared with untreated cells, whereas an opposite alternation was caused by TFPI2 knockdown (Fig. 6h).

### AP-1 regulated the transcriptional activity of TFPI2 in OGD/R-treated endothelial cells

Two GSE dataset analyses showed that subunits of transcription factor AP-1 were differentially expressed in ischemic samples. The expression profile of genes that encode proteins composed of AP-1 was displayed in the form of heat maps. We could easily observe that c-Jun, c-Fos, and FosL1 were upregulated in both GSE33725 and GSE97537 (Fig. 7a). Then western blot assay verified increased c-Jun and c-Fos protein levels and phosphorylated c-Jun (p-c-Jun) in the cerebral cortex after MCAO/R treatment. However, compared to the Sham group, the FosL1 expression in the MCAO/R group showed only slight changes (Fig. 7b). Thus, we next selected c-Jun or/and c-Fos to verify the transcriptionally regulatory role of AP-1 in TFPI2 through dual luciferase reporter assay. The sequence and location of the TFPI2 promoter that AP-1 might bind to were shown in Fig. 7c. And results from luciferase activity suggested that high

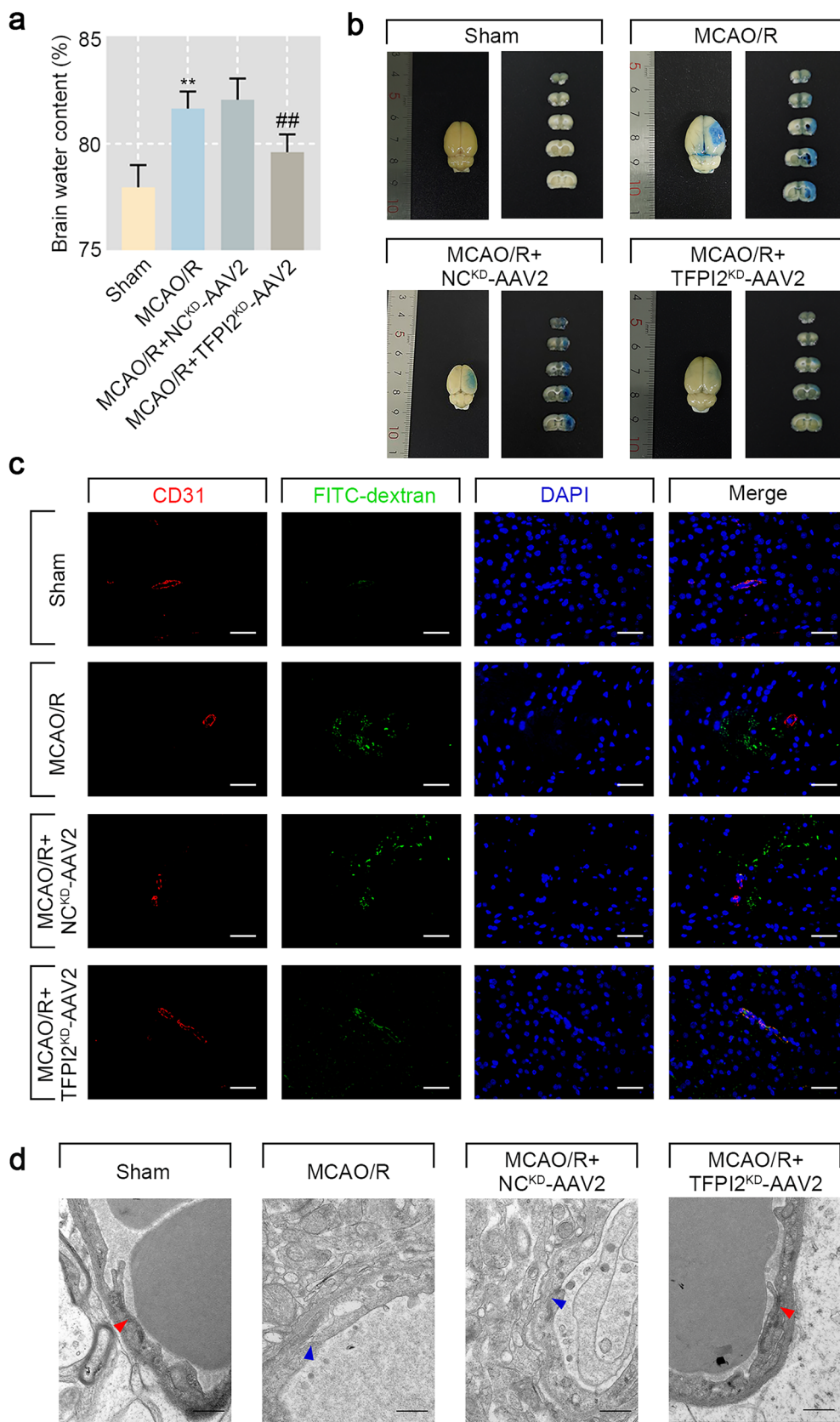




**Fig. 4** TFPI2 knockdown improves blood–brain barrier (BBB) integrity. **a** Brain-water content in brain tissues of rats ( $n=6$ ). **b** Evans blue extravasation in brain tissues of rats ( $n=6$ ). **c** FITC-dextran extravasation in brain tissues of rats and images of immunofluorescence staining locate endothelial cells ( $n=6$ ). Scale bar=50  $\mu\text{m}$ . **d** Images of transmission electron microscopy characterize tight junction (TJ) between endothelial cells ( $n=6$ ). Red arrows point out normal TJ while blue arrows point out abnormal TJ. Scale bar=500 nm.  $**p<0.01$  versus the Sham group,  $##p<0.01$  versus the MCAO/R + NC<sup>KD</sup>-AAV2 group

c-Jun or c-Fos expression elevated TFPI2 promoter activity compared with the empty vector group. Of note, compared with that, high co-expression of c-Jun and c-Fos had a higher relative luciferase activity (Fig. 7c). By measuring

the TFPI2 expression in bEnd.3 cells co-transfected with pcDNA3.1-c-Jun and pcDNA3.1-c-Fos plasmids, we found that TFPI2 mRNA and protein levels were greatly promoted by high co-expression of c-Jun and c-Fos (Fig. 7d, e). The siRNA-mediated c-Jun knockdown was conducted to inhibit the AP-1 activity in OGD/R-subjected bEnd.3 cells. A successful c-Jun knockdown was verified by the reduced c-Jun mRNA and protein level in OGD/R-subjected bEnd.3 cells after transfection with siRNA targeting c-Jun (Fig. 7f, g). The TFPI2 expression was significantly decreased following c-Jun knockdown (Fig. 7h, i).

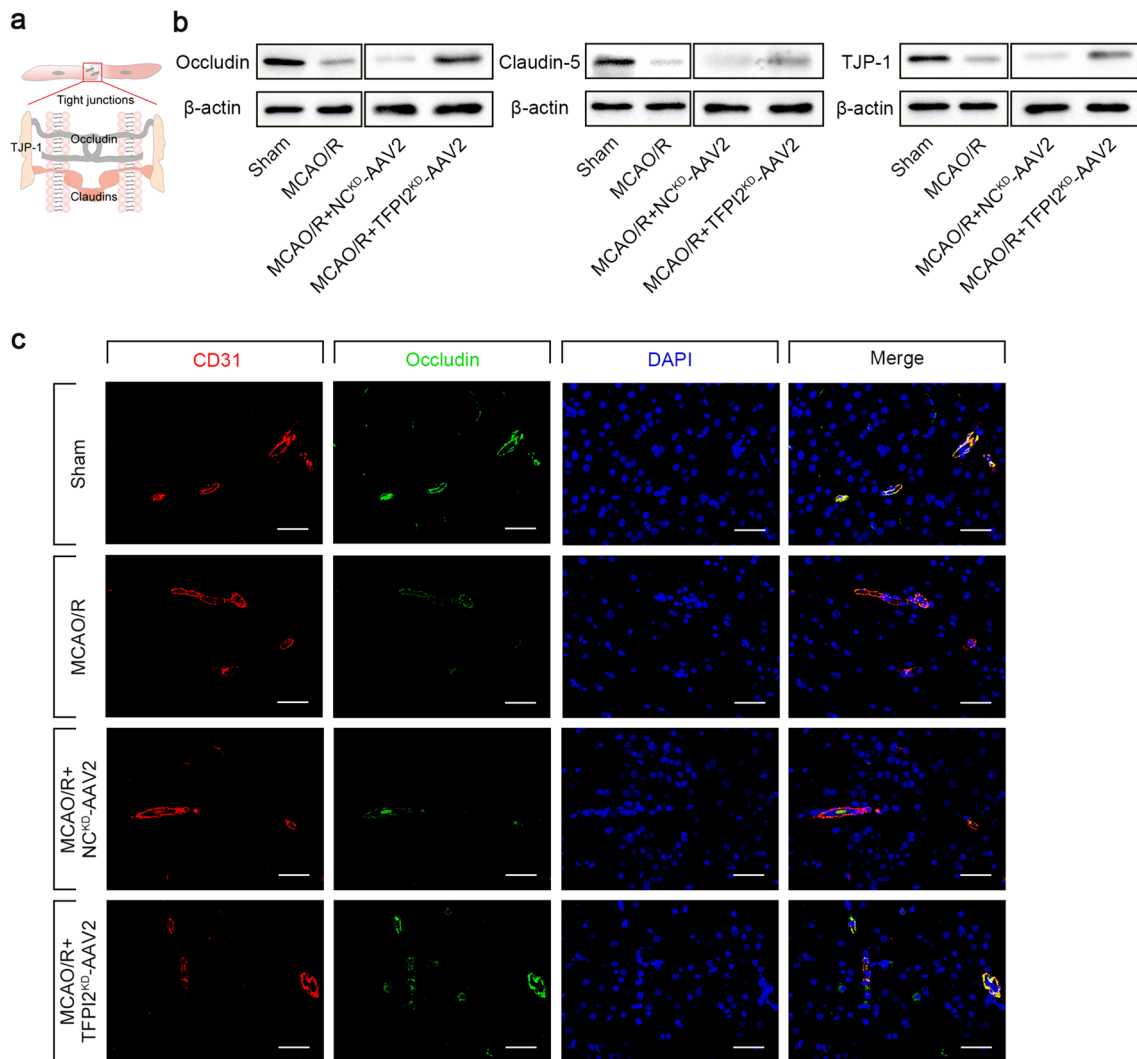


**Fig. 5** TFPI2 knockdown elevates the expression of TJ proteins. **a** The schematic diagram of the physical basis of BBB. **b** The protein levels of TJ proteins (Occludin, Claudin-5, TJP-1) in cerebral cortex of rats ( $n=6$ ). **c** Images of double immunofluorescence staining locate Occludin expression in endothelial cells ( $n=6$ ). Scale bar=50  $\mu\text{m}$

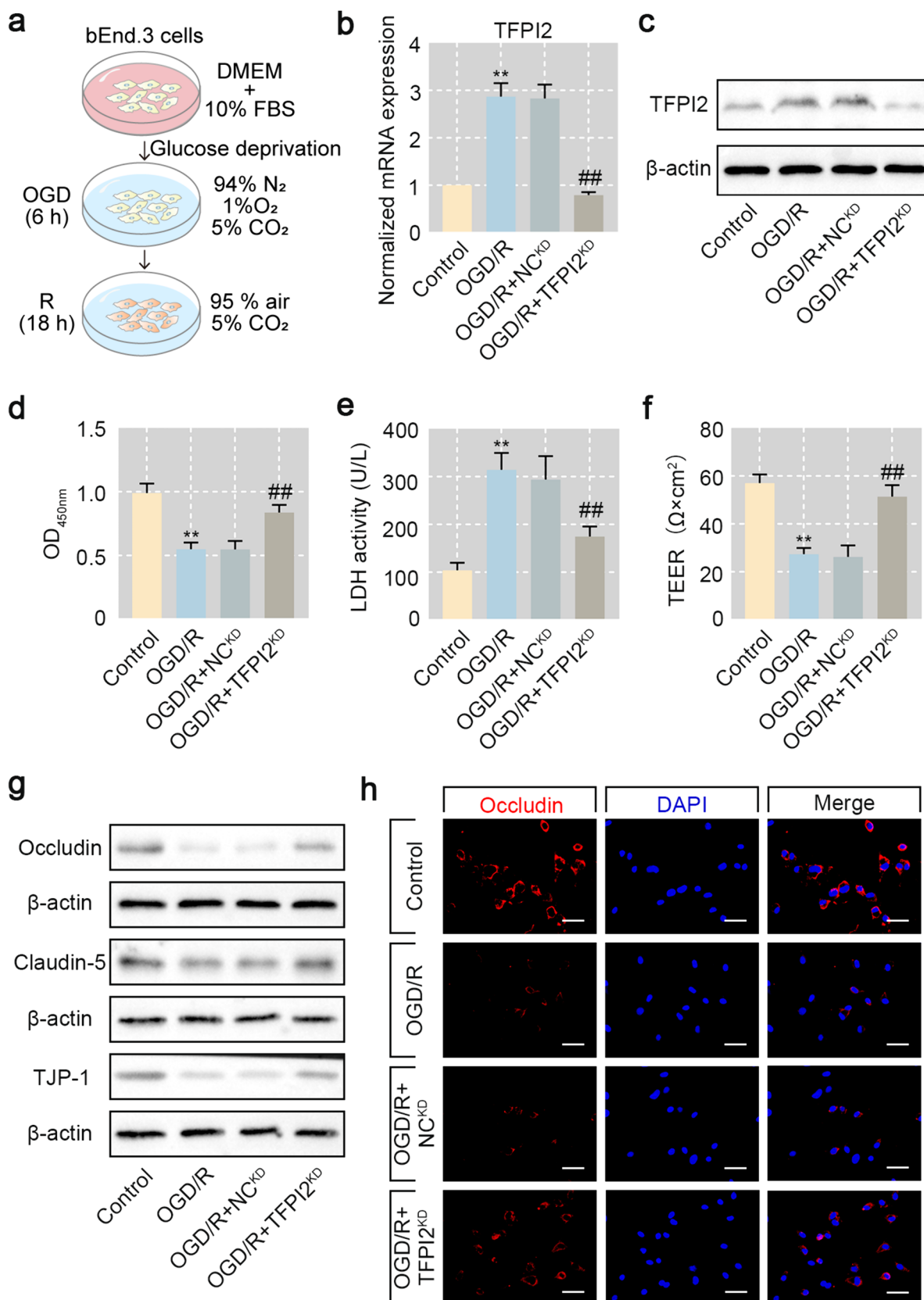


**Fig. 6** TFPI2 knockdown suppresses endothelial cell injury under the in vitro environment of CIRI. **a** The schematic diagram of mouse brain-driven Endothelial cells.3 (bEnd.3) cells exposed to oxygen and glucose deprivation (OGD) and reoxygenation (R) environment. **b** The mRNA expression of TFPI2 in bEnd.3 cells ( $n=3$ ). **c** The protein level of TFPI2 in bEnd.3 cells. **d** Cell viability of bEnd.3 cells indicated by CCK-8 assay ( $n=3$ ). **e** LDH activity in supernatant of bEnd.3 cell culture medium ( $n=3$ ). **f** TEER value reveals endothelial integrity of bEnd.3 cells ( $n=3$ ). **g** The protein levels of TJ proteins (Occludin, Claudin-5, TJP-1) in bEnd.3 cells ( $n=3$ ). **h** Images of immunofluorescence staining display Occludin expression in bEnd.3 cells ( $n=3$ ). Scale bar=50  $\mu\text{m}$ . \*\* $p < 0.01$  versus the Control group, ## $p < 0.01$  versus the OGD/R + NC<sup>KD</sup> group

## Discussion

Reperfusion following cerebral ischemia contributes to disrupted BBB integrity [27]. BBB is located at the interface between the blood and the brain tissues [28]. Brain microvascular endothelial cells combined with TJ and adherens junction constituted the physical basis of it [29]. Increased BBB permeability promotes adverse factors like cerebral inflammation and oxidative stress and in turn aggravates CIRI [30, 31]. In the current study, we set the BBB permeability as the entry point for alleviating CIRI. Based on this preset, TFPI2 was selected from upregulated DEGs derived from two GSE datasets. The effects of TFPI2 on CIRI and the underlying mechanism were subsequently clarified. For further exploration, we simulated CIRI in rats by MCAO/R surgery and bEnd.3 cells by OGD/R treatment.

So far, although TFPI2 has been extensively studied, the majority of them concentrated on the in vitro and in vivo models of cancers. GSE datasets showed that higher TFPI2 expression in the cerebral cortex of rats subjected to MCAO/R surgery was linked to CIRI, which provided a strong association between TFPI2 and CIRI. We also verified that rats had increased TFPI2 expression in the cerebral cortex following the MCAO/R operation. TFPI2 has been previously reported to inhibit angiogenesis. Chand et al. reported that TFPI2 secreted by tumor cells inhibited their malignant behaviors by playing a suppressive role in angiogenesis [32]. The increased angiogenesis was proposed to be along with the improvement in the BBB integrity [33]. Therefore, there was a possibility that the higher TFPI2 level downregulated endothelial cell angiogenesis and thereby took part in BBB disruption. Consistently, the increased TFPI2 in MEG8 silenced human umbilical vein endothelial cells was related to impaired angiogenic sprouting and endothelial function [16]. Similar to that previous evidence, we found that TFPI2 knockdown in bEnd.3 cells could alleviate endothelial cell damage following OGD/R treatment. Moreover, our results

revealed that TFPI2 knockdown increased the expression of TJ proteins (Occludin, Claudin-5, and TJP-1) in both rats and bEnd.3 cells with IRI. Colocalization of CD31 and TFPI2 in the cerebral cortex of rats revealed that TFPI2 was not only expressed in vascular endothelial cells. An online database (<http://betsholtzlab.org/VascularSingleCells/database.html>) showed that TFPI2 was expressed in pericytes, which are also cells in the cerebral cortex, of the adult mouse brain. Thus, TFPI2 might be expressed in pericytes in the cerebral cortex tissue, causing the staining of TFPI2 not completely to overlap with CD31. Our findings suggest that the effects of TFPI2 knockdown on CIRI were mediated by improved BBB integrity, including the alleviation of endothelial cell injury and the restoration of TJ, providing a new therapeutic target for CIRI treatment. However, we cannot rule out whether TFPI2 could affect MCAO/R by regulating other cells.

Increased LDH activity was found in the supernatant of bEnd.3 cells under the OGD/R condition and it was inhibited by TFPI2 knockdown. As a cytoplasmic enzyme, LDH could exert its roles during glycolysis such as regulating the conversion between lactate and pyruvate in the NAD-dependent manner [34]. It rapidly releases following the integrity of cell membranes is destroyed. Thus, LDH is a strong marker of the extent of cell damage. Ischemia is usually accompanied by oxygen deprivation of damaged tissues [35]. Under the hypoxia condition, anaerobic glycolysis increases and LDH catalyzes the conversion of pyruvate to lactate, causing tissue acidosis [36, 37]. Metabolic acidosis promotes the progression of inflammation. Furthermore, plenty of reactive oxygen species (ROS) are formed during reperfusion due to the re-induction of oxygen [38]. Both inflammation and ROS are risk factors for cell membrane disruption [39, 40]. Therefore, the increased LDH activity released by OGD/R-treated bEnd.3 cells might be related to inflammation and oxidative stress, which are considered to be important biologic processes during IRI [41]. Therefore, the effects of TFPI2 knockdown on the alleviation of OGD/R-induced endothelial cell injury might be partly mediated by downregulated inflammation and oxidative stress. However, we did not take inflammation and oxidative stress into consideration in the present study. The mechanism related to inflammation and oxidative stress underlying the role of TFPI2 in CIRI requires further elucidation.

According to GSE dataset analysis and JASPAR prediction, we believed that nuclear transcription factor AP-1 could regulate the transcription of TFPI2 and then affect the development of CIRI. By performing the dual luciferase reporter assay, we found that although high expression of c-Jun or c-Fos improved TFPI2 transcriptional activity, high

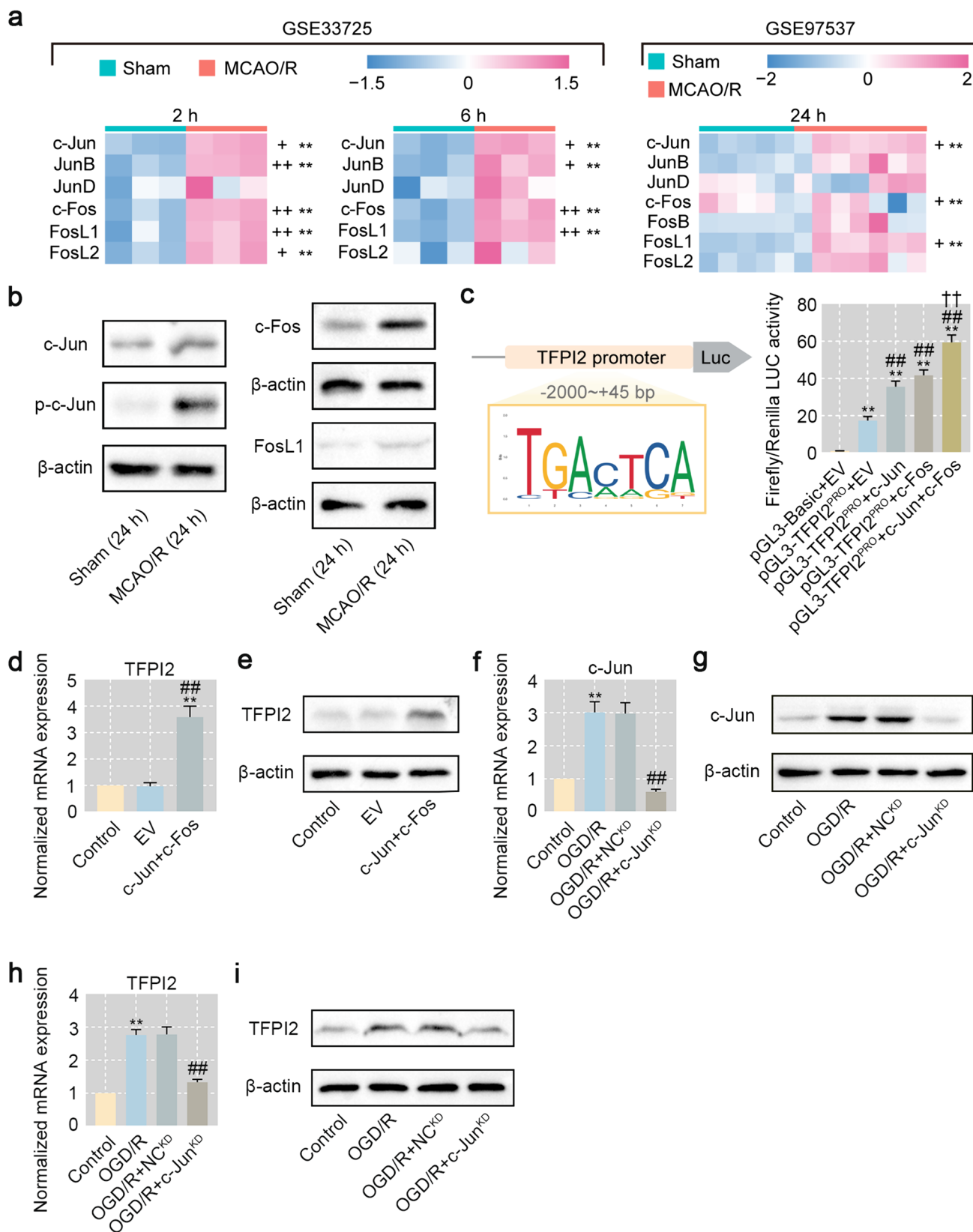


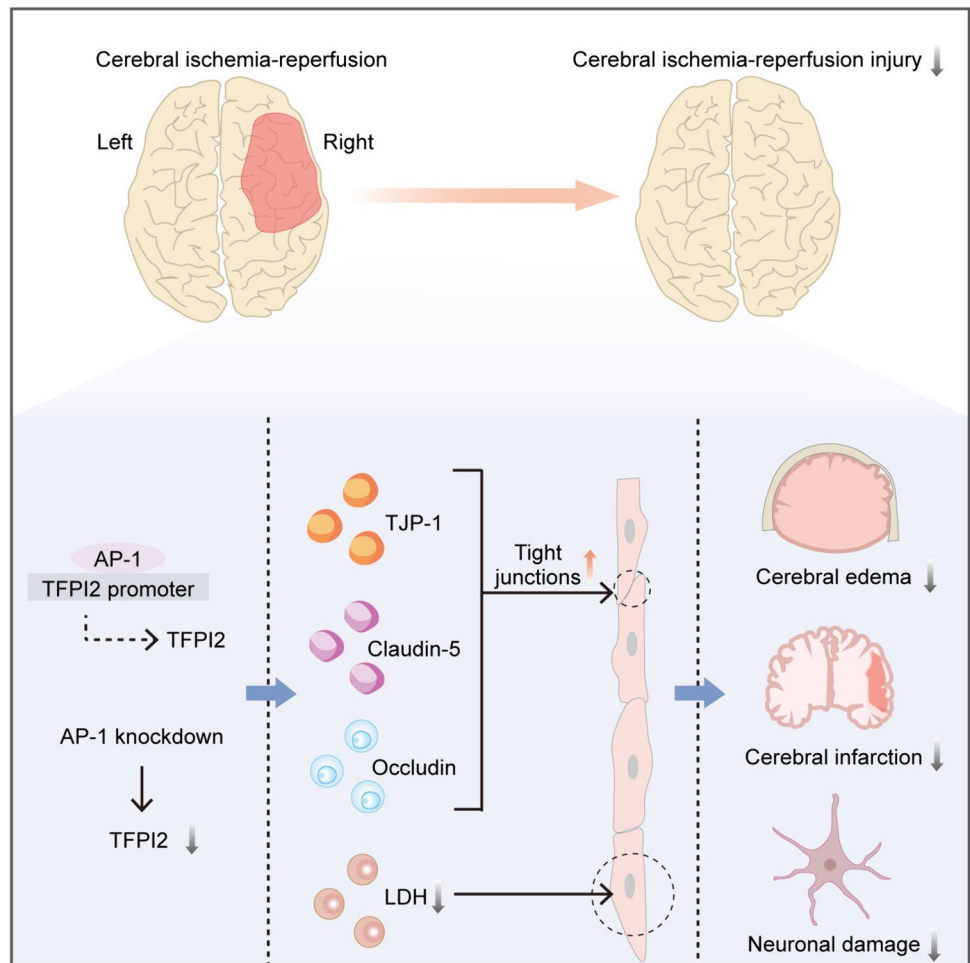
**Fig. 7** AP-1 regulates the TFPI2 transcription activity. **a** Heat maps show the expression profile of genes (c-Jun, JunB, JunD, c-Fos, FosB, FosL1, FosL2) encoding subunits of AP-1 complex from GSE33725 and GSE97537. + means  $1 < \text{Log}_2\text{FC} < 2$ , ++ means  $\text{Log}_2\text{FC} > 2$ , \*\* means  $p < 0.01$ . **b** The protein levels of c-Jun, c-Fos, and FosL1 in cerebral cortex of rats treated with sham operation or MCAO/R ( $n=3$ ). **c** The schematic diagram of possible binding sequences of AP-1 in the TFPI2 promoter region (left); TFPI2 promoter activity indicated by Firefly/Renilla luciferase (LUC) activity (right) ( $n=3$ ). **d** The mRNA expression of TFPI2 in bEnd.3 cells transfected with pcDNA3.1-c-Jun and pcDNA3.1-c-Fos (1:1) ( $n=3$ ). **e** The protein level of TFPI2 in bEnd.3 cells pcDNA3.1-c-Jun and pcDNA3.1-c-Fos (1:1) ( $n=3$ ). **f** The mRNA expression of c-Jun in bEnd.3 cells transfected with siRNA targeting c-Jun ( $n=3$ ). **g** The protein expression of c-Jun in bEnd.3 cells transfected with siRNA targeting c-Jun ( $n=3$ ). **h** The mRNA expression of TFPI2 in bEnd.3 cells transfected with siRNA targeting c-Jun ( $n=3$ ). **i** The protein level of TFPI2 in bEnd.3 cells transfected with siRNA targeting c-Jun ( $n=3$ ). \*\* $p < 0.01$  versus the pGL3-Basic+EV group or the Control group, ## $p < 0.01$  versus the pGL3-TFPI2<sup>PRO</sup>+EV group, the EV group, or the OGD/R+c-Jun<sup>KD</sup> group, and †† $p < 0.01$  versus the pGL3-TFPI2<sup>PRO</sup>+c-Jun group or the the pGL3-TFPI2<sup>PRO</sup>+c-Fos group

expression of the AP-1 complex (c-Jun and c-Fos) promoted the increase in the TFPI2 promoter activity to a greater

extent. Accordingly, it was the AP-1 complex that regulated the transcriptional activity of TFPI2, rather than just the subunits of the JUN or FOS family. There is a low affinity of c-Jun for DNA while high affinity of the AP-1 complex was found for the promoter of target genes [42], providing a certain support for results. Following that, loss of the c-Jun function in bEnd.3 cells was performed to partially inhibit the activity of the AP-1 complex. Decreased TFPI2 expression in OGD/R-treated bEnd.3 cells after c-Jun knockdown demonstrated the AP-1 complex was involved in CIRI by regulating TFPI2 transcriptional activity.

In summary, our study suggests that the high TFPI2 expression was associated with CIRI. TFPI2 knockdown restored BBB integrity by increasing the expression of TJ proteins and reducing endothelial cell injury, alleviating MCAO/R-induced CIRI. TFPI2 expression was transcriptionally regulated by AP-1. Our findings provide new evidence that the regulation of AP-1/TFPI2 axis could be used as a strategy to modulate BBB permeability, thereby affecting the development of CIRI (Fig. 8).

**Fig. 8** The AP-1/TFPI2 axis affects the development of CIRI





**Supplementary Information** The online version contains supplementary material available at <https://doi.org/10.1007/s13577-024-01125-3>.

**Author contributions** All authors contributed to the study conception and design. Material preparation, investigation, data collection were performed by Yue Cao, Ruixian Xing, and Xin Li. Formal analysis and visualization were performed by Qiushi Li, Yang Bai, and Xuewen Liu. The first draft of the manuscript was written by Yue Cao and Buxian Tian and revised by Xin Li. All authors read and approved the final manuscript.

**Funding** This study was funded by Tianjin Key Medical Discipline (Specialty) Construction Project (TJYXZDXK-065B).

**Data availability** The data generated in the current study are available from the corresponding author on reasonable request.

## Declarations

**Competing interests** The authors have no relevant financial or non-financial interests to disclose.

**Ethics approval** This study was performed in line with the principles of NIH Guide for the Care and Use of Laboratory Animals. Approval was granted by Institutional Animal Care and Use Committee of Tianjin Medical University (Approval Number: KY2020K192).

## References

- Xu J, Wang T, Guo F, Ji E, Zhang Y, Wu H, et al. Systematic identification of the protective effect of Danhong injection and BuChang NaoXinTong capsules on transcription factors in cerebral ischemia mice brain. *Oxid Med Cell Longev*. 2020;2020:5879852. <https://doi.org/10.1155/2020/5879852>.
- Kim DY, Zhang H, Park S, Kim Y, Bae CR, Kim YM, et al. CU06-1004 (endothelial dysfunction blocker) ameliorates astrocyte end-feet swelling by stabilizing endothelial cell junctions in cerebral ischemia/reperfusion injury. *J Mol Med (Berl)*. 2020;98(6):875–86. <https://doi.org/10.1007/s00109-020-01920-z>.
- Zeng X, Zhang Y-D, Ma R-Y, Chen Y-J, Xiang X-M, Hou D-Y, et al. Activated Drp1 regulates p62-mediated autophagic flux and aggravates inflammation in cerebral ischemia-reperfusion via the ROS-RIP1/RIP3-exosome axis. *Mil Med Res*. 2022;9(1):25. <https://doi.org/10.1186/s40779-022-00383-2>.
- Shen Z, Zheng Y, Wu J, Chen Y, Wu X, Zhou Y, et al. PARK2-dependent mitophagy induced by acidic postconditioning protects against focal cerebral ischemia and extends the reperfusion window. *Autophagy*. 2017;13(3):473–85. <https://doi.org/10.1080/15548627.2016.1274596>.
- Jurcau A, Simion A. Neuroinflammation in cerebral ischemia and ischemia/reperfusion injuries: from pathophysiology to therapeutic strategies. *Int J Mol Sci*. 2021. <https://doi.org/10.3390/ijms23010014>.
- Lv G, Wang GQ, Xia ZX, Wang HX, Liu N, Wei W, et al. Influences of blood lipids on the occurrence and prognosis of hemorrhagic transformation after acute cerebral infarction: a case-control study of 732 patients. *Mil Med Res*. 2019;6(1):2. <https://doi.org/10.1186/s40779-019-0191-z>.
- Yamazaki Y, Shinohara M, Shinohara M, Yamazaki A, Murray ME, Liesinger AM, et al. Selective loss of cortical endothelial tight junction proteins during Alzheimer's disease progression. *Brain*. 2019;142(4):1077–92. <https://doi.org/10.1093/brain/awz011>.
- Li S, Wang Y, Jiang D, Ni D, Kuttyreff CJ, Barnhart TE, et al. Spatiotemporal distribution of agrin after intrathecal injection and its protective role in cerebral ischemia/reperfusion injury. *Adv Sci (Weinh)*. 2020;7(4):1902600. <https://doi.org/10.1002/advs.201902600>.
- Miller JP, Holcomb J, Al-Ramahi I, de Haro M, Gafni J, Zhang N, et al. Matrix metalloproteinases are modifiers of huntingtin proteolysis and toxicity in Huntington's disease. *Neuron*. 2010;67(2):199–212. <https://doi.org/10.1016/j.neuron.2010.06.021>.
- Underly RG, Levy M, Hartmann DA, Grant RI, Watson AN, Shih AY. Pericytes as inducers of rapid, matrix metalloproteinase-9-dependent capillary damage during ischemia. *J Neurosci*. 2017;37(1):129–40. <https://doi.org/10.1523/jneurosci.2891-16.2016>.
- Shi Y, Zhang L, Pu H, Mao L, Hu X, Jiang X, et al. Rapid endothelial cytoskeletal reorganization enables early blood-brain barrier disruption and long-term ischaemic reperfusion brain injury. *Nat Commun*. 2016;7:10523. <https://doi.org/10.1038/ncomms10523>.
- Seanoon K, Payongsri P, Vivithanaporn P, Sirachainan N, Chuan-sumrit A, Hongeng S, et al. Mutations of TFPI-binding exosites on factor VII cause bleeding phenotypes in factor VII deficiency. *Blood Adv*. 2022;6(22):5887–97. <https://doi.org/10.1182/bloodadvances.2022007560>.
- Karmakar D, Maity J, Mondal P, Shyam Chowdhury P, Sikdar N, Karmakar P, et al. E2F5 promotes prostate cancer cell migration and invasion through regulation of TFPI2, MMP-2 and MMP-9. *Carcinogenesis*. 2020;41(12):1767–80. <https://doi.org/10.1093/carcin/bgaa043>.
- Guan G, Xie J, Dai Y, Han H. TFPI2 suppresses the interaction of TGF- $\beta$ 2 pathway regulators to promote endothelial-mesenchymal transition in diabetic nephropathy. *J Biol Chem*. 2022;298(3):101725. <https://doi.org/10.1016/j.jbc.2022.101725>.
- Ivanciu L, Gerard RD, Tang H, Lupu F, Lupu C. Adenovirus-mediated expression of tissue factor pathway inhibitor-2 inhibits endothelial cell migration and angiogenesis. *Arterioscler Thromb Vasc Biol*. 2007;27(2):310–6. <https://doi.org/10.1161/01.ATV.0000254147.89321.cf>.
- Kremer V, Bink DI, Stanicek L, van Ingen E, Gimbel T, Hilderink S, et al. MEG8 regulates tissue factor pathway inhibitor 2 (TFPI2) expression in the endothelium. *Sci Rep*. 2022;12(1):843. <https://doi.org/10.1038/s41598-022-04812-z>.
- Shibata S, Kashiwagi M, Morgan BA, Georgopoulos K. Functional interactions between Mi-2 $\beta$  and AP1 complexes control response and recovery from skin barrier disruption. *J Exp Med*. 2020. <https://doi.org/10.1084/jem.20182402>.
- Wang T, Jin X, Liao Y, Sun Q, Luo C, Wang G, et al. Association of NF- $\kappa$ B and AP-1 with MMP-9 overexpression in 2-chloroethanol exposed rat astrocytes. *Cells*. 2018. <https://doi.org/10.3390/cells7080096>.
- Shaulian E, Karin M. AP-1 as a regulator of cell life and death. *Nat Cell Biol*. 2002;4(5):E131–6. <https://doi.org/10.1038/ncb0502-e131>.
- Raivich G, Behrens A. Role of the AP-1 transcription factor c-Jun in developing, adult and injured brain. *Prog Neurobiol*. 2006;78(6):347–63. <https://doi.org/10.1016/j.pneurobio.2006.03.006>.
- Dai WJ, Funk A, Herdegen T, Unger T, Culman J. Blockade of central angiotensin AT(1) receptors improves neurological outcome and reduces expression of AP-1 transcription factors after focal brain ischemia in rats. *Stroke*. 1999;30(11):2391–8; discussion 8–9. <https://doi.org/10.1161/01.str.30.11.2391>.
- Zingarelli B, Hake PW, Yang Z, O'Connor M, Denenberg A, Wong HR. Absence of inducible nitric oxide synthase modulates



- early reperfusion-induced NF-kappaB and AP-1 activation and enhances myocardial damage. *Faseb j*. 2002;16(3):327–42. <https://doi.org/10.1096/fj.01-0533com>.
23. Zwacka RM, Zhang Y, Zhou W, Halldorson J, Engelhardt JF. Ischemia/reperfusion injury in the liver of BALB/c mice activates AP-1 and nuclear factor kappaB independently of IkappaB degradation. *Hepatology*. 1998;28(4):1022–30. <https://doi.org/10.1002/hep.510280417>.
  24. Kuts R, Frank D, Gruenbaum BF, Grinshpun J, Melamed I, Knyazer B, et al. A novel method for assessing cerebral edema, infarcted zone and blood-brain barrier breakdown in a single post-stroke rodent brain. *Front Neurosci*. 2019;13:1105. <https://doi.org/10.3389/fnins.2019.01105>.
  25. Longa EZ, Weinstein PR, Carlson S, Cummins R. Reversible middle cerebral artery occlusion without craniectomy in rats. *Stroke*. 1989;20(1):84–91. <https://doi.org/10.1161/01.str.20.1.84>.
  26. Lu H, Ashiqueali R, Lin CI, Walchale A, Clendaniel V, Matheson R, et al. Histone deacetylase 3 inhibition decreases cerebral edema and protects the blood-brain barrier after stroke. *Mol Neurobiol*. 2023;60(1):235–46. <https://doi.org/10.1007/s12035-022-03083-z>.
  27. Kim GS, Yang L, Zhang G, Zhao H, Selim M, McCullough LD, et al. Critical role of sphingosine-1-phosphate receptor-2 in the disruption of cerebrovascular integrity in experimental stroke. *Nat Commun*. 2015;6:7893. <https://doi.org/10.1038/ncomms8893>.
  28. André S, Larbanoix L, Verteneuil S, Stanicki D, Nonclercq D, Vander Elst L, et al. Development of an LDL receptor-targeted peptide susceptible to facilitate the brain access of diagnostic or therapeutic agents. *Biology (Basel)*. 2020. <https://doi.org/10.3390/biology9070161>.
  29. Goeritzer M, Bernhart E, Plastira I, Reicher H, Leopold C, Eichmann TO, et al. Myeloperoxidase and septic conditions disrupt sphingolipid homeostasis in murine brain capillaries in vivo and immortalized human brain endothelial cells in vitro. *Int J Mol Sci*. 2020. <https://doi.org/10.3390/ijms21031143>.
  30. Ma M, Hasegawa Y, Koibuchi N, Toyama K, Uekawa K, Nakagawa T, et al. DPP-4 inhibition with linagliptin ameliorates cognitive impairment and brain atrophy induced by transient cerebral ischemia in type 2 diabetic mice. *Cardiovasc Diabetol*. 2015;14:54. <https://doi.org/10.1186/s12933-015-0218-z>.
  31. Pan X, Fan J, Peng F, Xiao L, Yang Z. SET domain containing 7 promotes oxygen-glucose deprivation/reoxygenation-induced PC12 cell inflammation and oxidative stress by regulating Keap1/Nrf2/ARE and NF-κB pathways. *Bioengineered*. 2022;13(3):7253–61. <https://doi.org/10.1080/21655979.2022.2045830>.
  32. Chand HS, Du X, Ma D, Inzunza HD, Kamei S, Foster D et al. The effect of human tissue factor pathway inhibitor-2 on the growth and metastasis of fibrosarcoma tumors in athymic mice. *Blood*. 103(3):1069–77. <https://doi.org/10.1182/blood-2003-06-1930>.
  33. Mohamud Yusuf A, Hagemann N, Zhang X, Zafar M, Hussner T, Bromkamp C, et al. Acid sphingomyelinase deactivation post-ischemia promotes brain angiogenesis and remodeling by small extracellular vesicles. *Basic Res Cardiol*. 2022;117(1):43. <https://doi.org/10.1007/s00395-022-00950-7>.
  34. Gholipourmalekabadi M, Sameni M, Radenkovic D, Mozafari M, Mossahebi-Mohammadi M, Seifalian A. Decellularized human amniotic membrane: how viable is it as a delivery system for human adipose tissue-derived stromal cells? *Cell Prolif*. 2016;49(1):115–21. <https://doi.org/10.1111/cpr.12240>.
  35. Bertrand L, Méroth F, Tournebize M, Leda AR, Sun E, Toborek M. Targeting the HIV-infected brain to improve ischemic stroke outcome. *Nat Commun*. 2019;10(1):2009. <https://doi.org/10.1038/s41467-019-10046-x>.
  36. Viikilä P, Kivelä AJ, Mustonen H, Koskensalo S, Waheed A, Sly WS, et al. Carbonic anhydrase enzymes II, VII, IX and XII in colorectal carcinomas. *World J Gastroenterol*. 2016;22(36):8168–77. <https://doi.org/10.3748/wjg.v22.i36.8168>.
  37. Kwon YJ, Seo EB, Kwon SH, Lee SH, Kim SK, Park SK, et al. Extracellular acidosis promotes metastatic potency via decrease of the BMAL1 circadian Clock gene in breast cancer. *Cells*. 2020. <https://doi.org/10.3390/cells9040989>.
  38. Penna C, Femminò S, Caldera F, Rubin Pedrazzo A, Cecone C, Alfi E, et al. Cyclic nigerosyl-nigerose as oxygen nanocarrier to protect cellular models from hypoxia/reoxygenation injury: implications from an in vitro model. *Int J Mol Sci*. 2021. <https://doi.org/10.3390/ijms22084208>.
  39. Gu L, Sun M, Li R, Zhang X, Tao Y, Yuan Y, et al. Didymin suppresses microglia pyroptosis and neuroinflammation through the Asc/Caspase-1/GSDMD pathway following experimental intracerebral hemorrhage. *Front Immunol*. 2022;13: 810582. <https://doi.org/10.3389/fimmu.2022.810582>.
  40. Roselló-Busquets C, Hernaiz-Llorens M, Soriano E, Martínez-Mármol R. Nystatin regulates axonal extension and regeneration by modifying the levels of nitric oxide. *Front Mol Neurosci*. 2020;13:56. <https://doi.org/10.3389/fnmol.2020.00056>.
  41. Wu L, Xiong X, Wu X, Ye Y, Jian Z, Zhi Z, et al. Targeting oxidative stress and inflammation to prevent ischemia-reperfusion injury. *Front Mol Neurosci*. 2020;13:28. <https://doi.org/10.3389/fnmol.2020.00028>.
  42. Proctor CJ, Macdonald C, Milner JM, Rowan AD, Cawston TE. A computer simulation approach to assessing therapeutic intervention points for the prevention of cytokine-induced cartilage breakdown. *Arthritis Rheumatol*. 2014;66(4):979–89. <https://doi.org/10.1002/art.38297>.

**Publisher's Note** Springer Nature remains neutral with regard to jurisdictional claims in published maps and institutional affiliations.

Springer Nature or its licensor (e.g. a society or other partner) holds exclusive rights to this article under a publishing agreement with the author(s) or other rightsholder(s); author self-archiving of the accepted manuscript version of this article is solely governed by the terms of such publishing agreement and applicable law.